J. Fluid Mech. (1993), *vol.* 257, *pp.* 485–505

Copyright © 1993 Cambridge University Press

Feedback control stabilization of the no-motion state of a fluid confined in a horizontal porous layer heated from below

By JIE TANG AND HAIM H. BAU†

Department of Mechanical Engineering and Applied Mechanics, University of Pennsylvania, Philadelphia, PA 19104-6315, USA

(Received 25 January 1993 and in revised form 24 June 1993)

We consider a horizontal three-dimensional saturated porous layer, confined in an upright cubic box, heated from below and cooled from above. In the absence of a controller, the fluid maintains a no-motion state for subcritical Rayleigh numbers $R < R_c$, where R_c depends on the box's aspect ratio. Once this critical number is exceeded, fluid motion ensues. We demonstrate that, with the use of feedback control strategies which suppress flow instabilities, one can maintain a stable no-motion state for Rayleigh numbers far exceeding the classical critical one for the onset of convection. To preserve the equilibrium no-motion state of the classical problem, the controller alters the system's dynamics so as to stabilize an otherwise non-stable state.

1. Introduction

In many material processing applications, it may be desirable to operate at Rayleigh numbers higher than the one at which convection normally occurs and yet have no convection. Current alternatives for suppressing convection include the use of magnetic fields to damp fluid motion (an option limited to electrically conducting materials) and processing materials at reduced gravity in space to minimize the effect of buoyant convective currents. A considerable amount of work also has been devoted to delaying the onset of Rayleigh–Bénard convection in a horizontal fluid layer heated from below and cooled from above through the modulation of the boundary data. Most of these attempts have included the use of time-periodic modulation of the temperature difference across the layer (for lucid reviews, see Davis 1976 and Donnelly 1990). Unfortunately, this technique provides only a slight increase in the critical Rayleigh number (Meyer, Cannell & Ahlers 1992). Moreover, periodic modulation may lead to a subcritical bifurcation (Roppo, Davis & Rosenblat 1984), thereby causing the no-motion state to have only a limited basin of attraction. In other words, the no-motion state may be stable only for small disturbances. Recently, Kelly (1992) proposed delaying the onset of thermal convection by causing the fluid in the layer to oscillate slowly about a zero mean with two out-of-phase horizontal velocity components. Kelly predicts that the procedure may lead to substantial stabilization. However, his procedure may be difficult to implement in practice and the necessary horizontal motions may have adverse effects in materials processing applications.

In prior experimental and theoretical investigations (Singer, Wang & Bau 1991; Singer & Bau 1991; and Wang, Singer & Bau 1992), we used a feedback controller to successfully alter the bifurcation structure of convective motions in a thermal

† Author to whom correspondence should be addressed.

convection loop heated from below and cooled from above. For example, with the aid of a controller, we were able to delay the transition from a no-motion to a motion state, laminarize the naturally occurring chaotic motion in the loop for Rayleigh numbers far exceeding the one at the onset of chaos in the uncontrolled system, stabilize otherwise non-stable periodic orbits embedded in the chaotic attractor, and induce chaos under conditions in which the flow normally would be laminar.

Encouraged by our success with this work, we decided to implement similar ideas with a more complex thermal convective system, that of a horizontal saturated porous layer confined in a box, heated from below and cooled from above (the classic Lapwood 1948 problem). We chose the problem of Lapwood convection for study because of its relevance, among other things, to transport processes in the mushy region of solidification processes and in thermal porous insulators. In the latter case, one can envision 'active' insulators in which a controller is used to suppress convective currents, thereby reducing heat transfer. Still another reason for our choice of the Lapwood problem is that the saturated porous medium is a convenient medium for experimental verification of the concepts described in this paper. This is because the onset of convection in the porous case occurs at much higher temperature differences than it does in the Newtonian fluid case. Consequently, experiments in porous media can be conducted in a cruder and less expensive apparatus than would be required in the Newtonian fluid case.

We model the convection in porous media using the Darcy–Oberbeck–Boussinesq (DOB) equations. Prior experimental work (i.e. Katto & Masuoka 1967; and Bau & Torrance 1982) indicates that for low and moderate Darcy–Rayleigh numbers (R), the DOB equations adequately describe the convective processes in a saturated porous medium.

For low R-values, the classical DOB equations of motion admit a conduction (no-motion) solution which is globally stable for $R < R_c$, where R_c depends on the aspect ratio of the box (Beck 1972). Once this critical Rayleigh number is exceeded, steady motion ensues. By using feedback control strategies, we can maintain the no-motion state for Rayleigh numbers far exceeding the critical one. The controller does not alter the equilibrium, no-motion solution of the classical DOB equations. It only changes the system's stability characteristics by altering the system's dynamics.

2. A brief review of the classical Lapwood problem

Consider a horizontal homogeneous saturated porous layer confined in an upright box (figure 1). The box is uniformly heated from below and cooled from above. The side walls are insulated. We use, respectively, the height of the box H, the thermal diffusion time H^2/α (where α is the equivalent thermal diffusivity of the porous medium), and the nominal temperature difference between the bottom and top ΔT^* as the length, time and temperature scales. In the uncontrolled system, the non-dimensional bottom and top temperatures T are assigned the values one and zero, respectively. The non-dimensional, horizontal dimensions of the box are L_x and L_y. The motion of the fluid is described by the DOB equations (see Joseph 1976):

$$\frac{\partial \Xi}{\partial t} = F(\Xi; R), \tag{1}$$

where $\Xi(x, y, z, t)^T = \{\boldsymbol{u}, \theta\}$; $\boldsymbol{u}^T = \{u_x, u_y, u_z\}$ is the divergent-free ($\nabla \cdot \boldsymbol{u} = 0$), non-dimensional velocity vector which satisfies zero normal velocity on all solid surfaces; x and y are horizontal Cartesian coordinates; and z is the vertical coordinate. The top

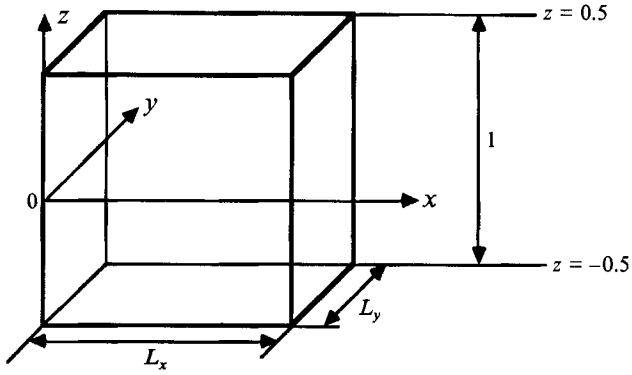

FIGURE 1. Schematic description of the saturated porous medium confined in a box of horizontal dimensions L_x and L_y.

and bottom boundaries are located at $z = \pm\frac{1}{2}$. In the absence of motion, the temperature distribution is $\frac{1}{2}-z$. $\theta(x, y, z, t) = T(x, y, z, t)-(\frac{1}{2}-z)$ is the deviation of the non-dimensional temperature from the linear (conduction) profile; $R = g\lambda\beta H\Delta T^*/\nu\alpha$ is the Darcy–Rayleigh number; g is the gravitational acceleration; λ is the medium's permeability; β and ν are, respectively, the thermal expansion coefficient and the kinetic viscosity of the saturating fluid; and F is the nonlinear operator:

$$F(\Xi; R) = \begin{cases} B^{-1}(-\boldsymbol{u}-\nabla p+R\theta\hat{\boldsymbol{e}}_z) \\ \chi^{-1}(u_z-\boldsymbol{u}\cdot\nabla\theta+\nabla^2\theta), \end{cases} \tag{2}$$

with the boundary conditions:

$$\left.\begin{aligned} &\theta(x, y, \pm\tfrac{1}{2}, t) = 0, \\ &\frac{\partial\theta(0, y, z, t)}{\partial x} = \frac{\partial\theta(L_x, y, z, t)}{\partial x} = \frac{\partial\theta(x, 0, z, t)}{\partial y} = \frac{\partial\theta(x, L_y, z, t)}{\partial y} = 0. \end{aligned}\right\} \tag{3}$$

In the above, p is the pressure deviation from its hydrostatic value; $B = (\lambda/\phi H^2)(\alpha/\nu)$ (usually, $B \ll 1$); ϕ is the porosity; and $\chi = (\rho_0 c_p)_{eq}/(\rho_0 c_p)_f$ is the ratio between the equivalent thermal capacity of the medium and that of the saturating fluid.

The equations for the linear stability of the no-motion state (see Beck 1972),

$$\left(B\frac{\partial}{\partial t}+1\right)\nabla^2 u_z' = R^{\frac{1}{2}}\nabla_1^2\theta, \quad \left(\chi\frac{\partial}{\partial t}-\nabla^2\right)\theta = R^{\frac{1}{2}}u_z', \tag{4}$$

are obtained by assuming the disturbance quantities $\{\boldsymbol{u}, \theta\}$ are small and by neglecting second-order terms in (2). In (4),

$$\boldsymbol{u}' = R^{\frac{1}{2}}\boldsymbol{u}, \quad \nabla_1^2 = \frac{\partial^2}{\partial x^2}+\frac{\partial^2}{\partial y^2}, \quad \nabla^2 = \nabla_1^2+\frac{\partial^2}{\partial z^2}.$$

The boundary conditions for θ are given in (3) and $u_z'(x, y, -\frac{1}{2}, t) = u_z'(x, y, \frac{1}{2}, t) = 0$. Next, the dependent variables are decomposed into normal modes,

$$u_z' = \sum_{n,m=1}^{\infty} f_{n,m}(x, y)\, W_{n,m}(z)\, e^{\sigma t}, \quad \theta = \sum_{n,m=1}^{\infty} f_{n,m}(x, y)\, \Theta_{n,m}(z)\, e^{\sigma t}, \tag{5}$$

where $f_{n,m}(x, y)$ are orthonormal functions satisfying the equation

$$\nabla_1^2 f_{n,m}+\kappa_{n,m}^2 f_{n,m} = 0 \tag{6}$$

with the boundary conditions

$$\frac{\partial f_{n,m}(0,y)}{\partial x} = \frac{\partial f_{n,m}(L_x,y)}{\partial x} = \frac{\partial f_{n,m}(x,0)}{\partial y} = \frac{\partial f_{n,m}(x,L_y)}{\partial y} = 0. \tag{7}$$

Equations (6) and (7) suggest that

$$f_{n,m}(x,y) = \cos(\kappa_{x,n}\, x)\cos(\kappa_{y,m}\, y),$$

where

$$\kappa_{n,m}^2 = \kappa_{x,n}^2 + \kappa_{y,m}^2 = \left(\frac{n\pi}{L_x}\right)^2 + \left(\frac{m\pi}{L_y}\right)^2,$$

and m and n are integers (one of which, but not both, may be zero). For example, $(n,m) = (1,0)$ or $(0,1)$ corresponds to a single, two-dimensional roll and $(n,m) = (1,1)$ corresponds to a three-dimensional, single cell. Upon substituting u_z' and θ into (5), we obtain

$$(\sigma B+1)(\mathrm{D}^2-\kappa_{n,m}^2)\, W_{n,m} = -\kappa_{n,m}^2 R^{\frac{1}{2}}\Theta_{n,m}, \quad (\mathrm{D}^2-\kappa_{n,m}^2-\chi\sigma)\,\Theta_{n,m} = -R^{\frac{1}{2}}W_{n,m}, \tag{8}$$

where $\mathrm{D} = \mathrm{d}/\mathrm{d}z$. This set of differential equations can be reduced to the single equation

$$(\mathrm{D}^2-\kappa_{n,m}^2)(\mathrm{D}^2-\kappa_{n,m}^2-\chi\sigma)\,\Theta_{n,m} = \kappa_{n,m}^2 R\Theta_{n,m}, \tag{9}$$

with the isothermal and impermeable boundary conditions

$$\Theta_{n,m}(\tfrac{1}{2}) = \Theta_{n,m}(-\tfrac{1}{2}) = D^2\Theta_{n,m}(\tfrac{1}{2}) = \mathrm{D}^2\Theta_{n,m}(-\tfrac{1}{2}) = 0. \tag{10}$$

Since, for most porous materials, $B \ll 1$, we assumed above that $B = 0$. For a given R-value, (9)–(10) constitute an eigenvalue problem for the growth rate $\sigma = \sigma_R + \mathrm{i}\sigma_I$. We order σ in a descending sequence according to the magnitude of the eigenvalues' real parts with the eigenvalue with the largest real part denoted as σ_1. The sign of the real part of σ_1 determines the stability characteristics of the no-motion state. For $\sigma_{R,1} < 0$, the no-motion state is linearly stable. The marginal stability condition is obtained by determining the Rayleigh number which corresponds to growth rate $\sigma_{R,1} = 0$. Since (9)–(10) are self-adjoint, all values of σ are real and the marginal stability condition can be determined by setting $\sigma = 0$ in (9), which now becomes an eigenvalue problem for R. Equations (9)–(10) admit the even, $\cos[(2l+1)\pi z]$, and odd, $\sin(2l\pi z)$, eigenfunctions, where l is an integer. These eigenfunctions are proportional to the deviation of the vertical temperature profile from its conductive value at the onset of convection. The odd modes have a node (assume zero value) at the box's midheight ($z = 0$). The even and odd modes lose stability at different Rayleigh numbers. For example, for the cases of an infinite fluid layer, a cubic box ($L_x = L_y = 1$), and a square, the Rayleigh numbers for the onset of even and odd convective modes are, respectively, $4\pi^2$ and $16\pi^2$. Thus, in all the aforementioned cases, one would observe even modes at the onset of convection. The no-motion state's loss of stability occurs through a supercritical bifurcation into time-independent, cellular motion. For $R < R_c$, the no-motion solution, $\Xi = 0$, is globally stable (Joseph 1976).

3. Stabilization of the no-motion state

Our objective is to maintain the no-motion state for $R > R_c$ with the aid of a feedback controller consisting of sensors and actuators. The sensors will measure the temperature at a number of points inside the fluid and the actuators will react to any

deviation of the fluid's temperature from the desired conductive values by modifying the temperature at certain locations along the bottom of the box in such a way as to dissipate these deviations. Advances in microfabrication technology make it feasible, if necessary, to equip the box's bottom with a relatively large number of actuators at a reasonable cost. Thermal sensors and actuators appear to be the most convenient type of sensors and actuators to use for this particular application; but they are not the only type possible.

To aid in understanding the action of the controller, we briefly state the mechanisms responsible for the loss of stability of the no-motion state in the classical problem. The no-motion state is an equilibrium state for all Rayleigh numbers. As a result of random disturbances, the temperature in the fluid may deviate from its conductive value. Such a deviation will provide a buoyant force which, in turn, will induce fluid motion. For subcritical Rayleigh numbers, the induced motion is sufficiently slow to allow ample time for thermal conduction to dissipate any disturbances, remove the resulting buoyant forces, and restore the no-motion state. Our controller will act to assist these dissipative mechanisms.

More specifically, the sensors will detect any deviations in the temperature of the fluid from its conductive value and direct the actuators to reduce/increase slightly the bottom temperature beneath an ascending/descending fluid column. Through this action, the buoyant force will be reduced, thereby increasing the time available for the conduction to dissipate disturbances before they have the opportunity to manifest themselves. Once the disturbances have been dissipated, the bottom temperature is restored to its nominal, uniform, non-dimensional value of one. As we shall demonstrate later in the paper, by assisting the dissipative mechanisms, the controller allows a significant increase in the critical Rayleigh number for the onset of convection at the cost, typically, of only small modifications in the bottom temperature and thereby stabilize the no-motion state for some supercritical Rayleigh numbers.

Next, we present our feedback control strategy in mathematical form. Briefly, we propose to augment the dynamic system (1) with the controller $C(\cdot)$:

$$\frac{\partial \Xi}{\partial t} = G(\Xi; R) = F(\Xi; R) + C(\Xi; R, K), \tag{11}$$

where $C(0; R, K) = 0$ for all R- and K-values; and K is the controller's gain vector. Here, Ξ is the deviation of the measured variables from their desired value ($\Xi = 0$ in our case); and C may be either a linear or a nonlinear operator. Linear $C(\cdot)$ may represent proportional ($\mathbb{P}$), integral ($\mathbb{I}$), or differential ($\mathbb{D}$) control or some combination thereof (i.e. $\mathbb{PID}$). Note that the no-motion solution ($\Xi = 0$) is an equilibrium state of *both* the uncontrolled and the controlled systems. In other words, the controller does not alter the state we wish to stabilize; it only changes its stability characteristics.

Let us begin by assuming that the temperature distribution at some horizontal cross-section, i.e. $\theta_0 = \theta(x, y, 0, t)$ at $z = 0$, is known (or can be reconstructed) as a continuous function of the horizontal coordinates (x, y). Knowledge of the temperature profile is assumed for mathematical convenience and it may not be necessary for the practical application of the controller. Indeed, numerical experiments suggest that knowledge of the temperature at a few discrete points will suffice for successful application of the controller.

In the absence of motion, $\theta(x, y, z, t) = 0$ everywhere. When disturbances in the temperature field occur, fluid motion ensues and θ_0 deviates from its zero, conductive value. To suppress this fluid motion, the controller modifies momentarily the base's

temperature distribution in proportion to the measured deviation and its time derivative, i.e.

$$\theta(x, y, -\tfrac{1}{2}) = C(\theta_0) = -K_P \theta_0 - K_D \frac{\partial \theta_0}{\partial t}, \tag{12}$$

where K_P and K_D represent, respectively, the gains of proportional and differential controllers. Note that the controller reduces/increases slightly the base temperature at locations where the fluid tends to ascend/descend. Once the disturbance has disappeared, $\theta(x, y, -\frac{1}{2})$ will be restored to its nominal, zero value which is the same as in the uncontrolled case. Since, under normal operating conditions, the controller reacts to disturbances before they have an opportunity to grow, the alterations in the bottom's temperature will typically be small. We shall demonstrate in the next sections that this simple strategy can shift significantly the bifurcation point for the transition from the no-motion to the motion state.

4. Linear stability analysis

The linear stability analysis proceeds along the same lines as the classical analysis described in §2 with the exception that boundary condition (12) replaces the boundary condition $\theta(x, y, -\frac{1}{2}, t) = 0$ of the uncontrolled problem. The eigenvalue problem consists of (9) with the boundary conditions

$$\Theta_{n,m}(\tfrac{1}{2}) = \mathrm{D}^2\Theta_{n,m}(\tfrac{1}{2}) = \Theta_{n,m}(-\tfrac{1}{2}) + (K_P + \sigma K_D)\,\Theta_{n,m}(0)$$
$$= (\mathrm{D}^2 - \kappa_{n,m}^2 - \chi\sigma)\,\Theta_{n,m}(-\tfrac{1}{2}) = 0. \tag{13}$$

In the controlled case of $K_P > 0$ and/or $K_D > 0$, the analysis is a bit more complicated than in the classical problem because the application of the controller (13) breaks the symmetry in the boundary conditions. The system (9) and (13) is no longer self-adjoint, and the eigenvalues (σ), which correspond to the growth rate, are not guaranteed to be real. Consequently, the possibility of bifurcation from a no-motion state into time-dependent convection cannot be excluded. To obtain the conditions of marginal stability, we need to seek values of both R and $\sigma_{I,1}$ with $\sigma_{R,1} = 0$ such that (9) and (13) are non-trivially satisfied.

We start the analysis by investigating the dependence of the critical Rayleigh number on the proportional controller's gain (K_P) for $K_P \ll 1$ and $K_D = 0$. The smallness of K_P allows us to proceed with a perturbation analysis.

4.1. *Perturbation expansion* ($K_P \ll 1, K_D = 0$)

Consider R, σ_1, and Θ to be functions of K_P. Below, for conciseness, we drop all subscripts except those which denote the order of the approximation. We expand σ, R, and Θ into the corresponding Taylor series in terms of K_P about $K_P = 0$, i.e.

$$\sigma = \sigma_0 + \sigma_1 K_P + \sigma_2 K_P^2 + \ldots, \quad R = R_0 + K_P R_1 + K_P^2 R_2 + \ldots,$$
$$\Theta = \Theta_0 + \Theta_1 K_P + \Theta_2 K_P^2 + \ldots.$$

The resulting problem for $O(K_P^0)$ is identical to the classical Darcy–Rayleigh–Bénard problem, where the operator in (9) is self-adjoint. This implies $\sigma_0 = 0$; $R_0 = (\pi^2 + \kappa^2)^2/\kappa^2$ and $\Theta_0 = \cos(\pi z)$, where κ is the value which yields a minimum for R_0.

At higher orders of K_P, i.e. $O(K_P^l)$ with $l > 0$, we obtain a set of linear non-homogeneous equations of the form

$$[(\mathrm{D}^2-\kappa^2)^2-R_0\kappa^2]\,\Theta_l = \sum_{j=1}^{l}(\chi(\mathrm{D}^2-\kappa^2)\sigma_j+\kappa^2 R_j)\,\Theta_{l-j} \tag{14}$$

with the boundary conditions:

$$\Theta_l(\tfrac{1}{2}) = \Theta_l(-\tfrac{1}{2})+\Theta_{l-1}(0) = (\mathrm{D}^2-\kappa^2)\,\Theta_l(-\tfrac{1}{2})-\sum_{j=1}^{l}\chi\sigma_j\,\Theta_{l-j}(-\tfrac{1}{2}) = \mathrm{D}^2\Theta_l(\tfrac{1}{2}) = 0. \tag{15}$$

Since the null space of the linear operator in (14) is not empty, for solutions to exist the solvability condition (Fredholm's alternative),

$$\Theta_{l-1}(0)\,\pi[\pi^2+\kappa^2] = \sum_{j=1}^{l}\int_{-\frac{1}{2}}^{\frac{1}{2}}\Theta_0(z)[-\mathrm{i}\chi\sigma_{I,j}(\pi^2+\kappa^2)+\kappa^2 R_j]\,\Theta_{l-j}(z)\,\mathrm{d}z, \tag{16}$$

must be satisfied and we require that at marginal stability $\sigma_{R,j} = 0$.

Equation (16) suggests that $R_1 = 2\pi R_0/(\pi^2+\kappa^2)$ and $\sigma_{I,j} = 0$ for all j. That is, at criticality, $R = R_0+K_P R_1+O(K_P^2)$. The controller has the effect of increasing the value of the Rayleigh number at the onset of convection. For small values of K_P, the growth rates are real and the principle of exchange of stability holds. That is, the branch of $\sigma(K_P, R)$ which satisfies $\sigma(0, R_0) = 0$ is real. This, however, does not preclude the possibility that, as K_P increases, other branches of σ, possibly consisting of complex values, may dictate stability. As we shall see later (i.e. figures 6 and 7), this is, indeed, the case for $K_P > 3.85$.

Note that as long as the loss of stability occurs through a real eigenvalue ($\sigma = 0$ at the marginal stability), the differential controller (K_D) cannot shift the marginal stability curve to higher R-values. It may, however, have an impact on the system's dynamics.

4.2. *Stability analysis for any controller's gains*

For any values of K_P and K_D, we solve (9) and (13) directly. Equation (9) is satisfied by

$$\Theta(z) = A_1\cosh(x_1 z)+A_2\cos(x_2 z)+A_3\sinh(x_1 z)+A_4\sin(x_2 z), \tag{17}$$

where $x_1 = (\kappa^2+\frac{1}{2}(\chi\sigma+\tau))^{\frac{1}{2}}$, $x_2 = (-\kappa^2+\frac{1}{2}(-\chi\sigma+\tau))^{\frac{1}{2}}$, $\tau = (\chi^2\sigma^2+4\kappa^2 R)^{\frac{1}{2}}$.

By satisfying the boundary conditions (13), we obtain a set of four homogeneous linear algebraic equations for the coefficients A_i. For these equations to be non-trivially satisfied, it is necessary that the matrix

$$\begin{pmatrix} \boldsymbol{C} & \boldsymbol{D} \\ \boldsymbol{E} & \boldsymbol{0} \end{pmatrix} \tag{18}$$

be singular. In the above,

$$\boldsymbol{C} = \begin{pmatrix} 0 & \cos(\frac{1}{2}x_2) \\ \cosh(\frac{1}{2}x_1) & 0 \end{pmatrix}, \quad \boldsymbol{D} = \begin{pmatrix} 0 & \sin(\frac{1}{2}x_2) \\ \sinh(\frac{1}{2}x_1) & 0 \end{pmatrix},$$

$\boldsymbol{0}$ is a 2×2 matrix with all its entries being zero,

$$\boldsymbol{E} = \begin{pmatrix} K+2\cosh(\frac{1}{2}x_1) & K+2\cos(\frac{1}{2}x_2) \\ (\tau-\frac{1}{2}\chi\sigma)\cosh(\frac{1}{2}x_1) & -(\tau+\frac{1}{2}\chi\sigma)\cos(\frac{1}{2}x_2) \end{pmatrix},$$

and $K = K_P+\sigma K_D$. For the matrix (18) to be singular, we need either $\mathrm{Det}[\boldsymbol{D}] = 0$ or $\mathrm{Det}[\boldsymbol{E}] = 0$.

Just as in the case of the classical problem, $\mathrm{Det}[\boldsymbol{D}] = 0$ corresponds to loss of stability through odd modes (the corresponding eigenfunction is $\sin[x_2 z]$). For a cube, this loss of stability occurs at $R = 16\pi^2$. Our chosen control strategy has no effect on the odd modes. This is because our sensors are located at midheight, where the odd modes have a node. In order to stabilize the odd modes, we would need to place sensors at other heights where the odd modes do not have nodes, a set-up which we do not address in this paper. The control strategy discussed in this paper will be able to shift the bifurcation point only up to the Rayleigh number at which the odd modes are destabilized. In other words, in the case of a cubic box, the most we can hope for from our controller is to shift the loss of stability from $R = 4\pi^2$ to $R = 16\pi^2$. However, our chosen control strategy does have the advantage that the determinant (18) can still be factored, which, of course, simplifies the analysis.

The controller clearly affects the stability characteristics of the classical 'even modes'. Because the controller breaks the symmetry of the problem, in the presence of the controller, these modes are no longer even. The 'non-odd' eigenfunctions have the form

$$\Theta(z) = \left(\frac{2\cos(\frac{1}{2}x_2)+K}{2\cosh(\frac{1}{2}x_1)+K}\right)\frac{\sinh(x_1(z-\frac{1}{2}))}{\sinh(\frac{1}{2}x_1)} - \frac{\sin(x_2(z-\frac{1}{2}))}{\sin(\frac{1}{2}x_2)}. \tag{19}$$

The critical Rayleigh number for the onset of convection through eigenfunction (19) is obtained by solving the characteristic equation $\mathrm{Det}[\boldsymbol{E}] = 0$ or explicitly,

$$M(R,\sigma) = M_R + \mathrm{i}M_I = K(\tau+\tfrac{1}{2}\chi\sigma)\cos(\tfrac{1}{2}x_2) + K(\tau-\tfrac{1}{2}\chi\sigma)\cosh(\tfrac{1}{2}x_1) + 4\tau\cosh(\tfrac{1}{2}x_1)\cos(\tfrac{1}{2}x_2) = 0 \tag{20}$$

for R and σ_I with $\sigma_R = 0$.

One way to calculate solutions for (20) is to separate the equation into its imaginary and real parts and solve the simultaneous system $M_R(R,\sigma_I) = M_I(R,\sigma_I) = 0$ for R and σ_I. We used both *Mathematica's* (Wolfram 1991) root solver and the bifurcation software AUTO to calculate R and σ_I as functions of K_P, K_D, and the wavenumber κ. These methods trace efficiently a solution branch which corresponds to the classical stability limit at $K = 0$. These methods may not locate isolated solution branches, however.

In order to verify that for a given set (R, K_P, K_D, κ) no values of σ exist with a positive real part, we use the Nyquist criterion (Carrier, Krook & Pearson 1966). Briefly, the criterion states that the number of roots of (20) within a given closed curve (Σ) in the complex σ-plane is equal to the number of times $M(R,\sigma)$ encircles the origin of the complex M-plane as σ traverses Σ. $M(R,\sigma)$ must be analytic within and non-zero on Σ. We construct the curve Σ to consist (see insert in figure 2) of the imaginary axis and a half-circle whose radius can be enlarged to include the entire right-hand side of the complex σ-plane. Then we map the curve Σ from the complex σ-plane to the complex M-plane.

The function $M(R,\sigma)$, as given by (20), is not convenient to work with because the mapping of the large half-circle results in infinite numbers of partial encirclings of the origin in the M-plane. To overcome this difficulty, instead of investigating the locus of the roots of $M(R,\sigma)$, we work with the modified function

$$G(R,\sigma) = G_R + \mathrm{i}G_I = \tau^{-1}M(R,\sigma)\exp\{-\tfrac{1}{2}[\chi(\sigma+1)]^{\frac{1}{2}}\}, \tag{21}$$

which maps the half-circle at infinity to the point $2\cosh(\frac{1}{2}\kappa)$ on the positive (G_R) axis. In (21), we removed through division the non-consequential imaginary zeros of the function $M(R,\sigma)$. Otherwise, the zeros of $G(R,\sigma)$ are identical to those of $M(R,\sigma)$.

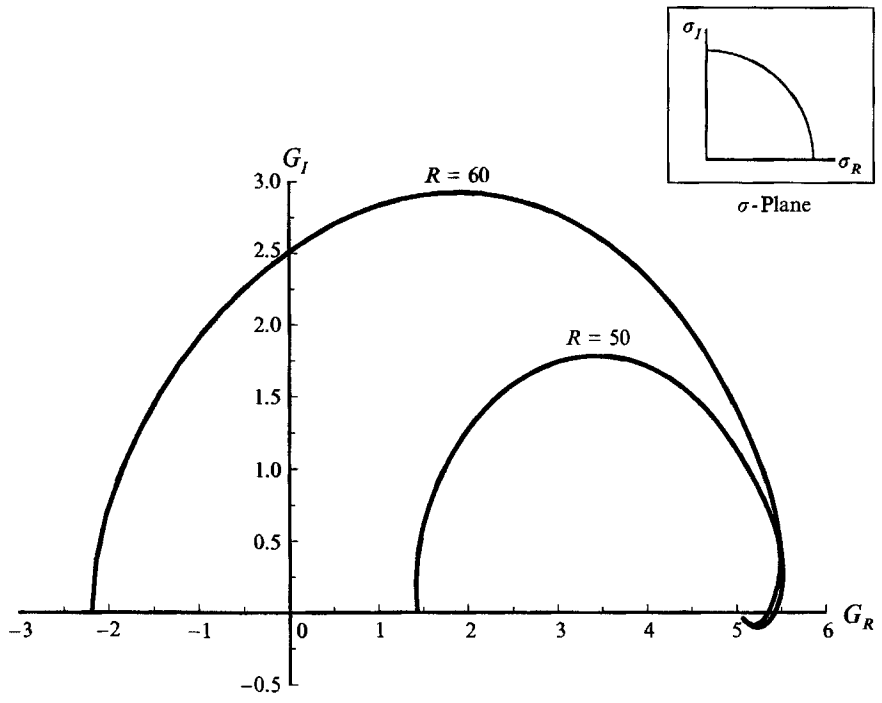

FIGURE 2. Nyquist diagram for $R = 50$ (stable case; the map in the G-plane does not encircle the origin) and $R = 60$ (non-stable case; the map in the G-plane encircles the origin once). $K_P = 1$, $K_D = 0$ and $(n, m) = (1, 0)$. The insert shows the contour Σ in the complex σ-plane.

All the calculations presented in this paper are for $L_x = L_y = 1$ and $\chi = 0.5$. Representative samples of the upper half of the Nyquist plots for stable and non-stable cases and for $K_D = 0$ and $(n, m) = (1, 0)$ are depicted, respectively, in figure 2 ($K_P = 1$, $R = 50$ and $R = 60$) and figure 3 ($K_P = 4$, $R = 133$). The curves are to be completed by their mirror images with respect to the real axis (G_R). Observe that the curve corresponding to $R = 50$ (figure 2) does not encircle the origin while the curve corresponding to $R = 60$ encircles the origin once, which implies the existence of a single root with a positive real part for $G(R, \sigma) = 0$. The no-motion state is stable at $R = 50$ and unstable at $R = 60$. Since complex roots will always come in pairs (as complex conjugates), this root must be real. Thus, the condition for a bifurcation through a single eigenvalue is that $G(R, 0)$ must cross from the positive to the negative part of the real axis. The marginal stability condition corresponds to $G(R, 0) = 0$. This criterion is true only for $K_P < 3.85$. For larger values of K_P, bifurcation occurs through a complex-conjugate pair.

In figure 3, we show the Nyquist diagram for $K_P = 4$ and $R = 133$. In this case, there is a complex-conjugate pair with a positive real part. Accordingly, the Nyquist map encircles the origin twice. The loss of stability is strict ($\mathrm{d}\sigma_R/\mathrm{d}R > 0$). Numerical experiments, which we describe later, suggest that this bifurcation is supercritical and leads to a stable limit cycle.

The marginal stability limits as a function of the controller's gains are reported in §6.

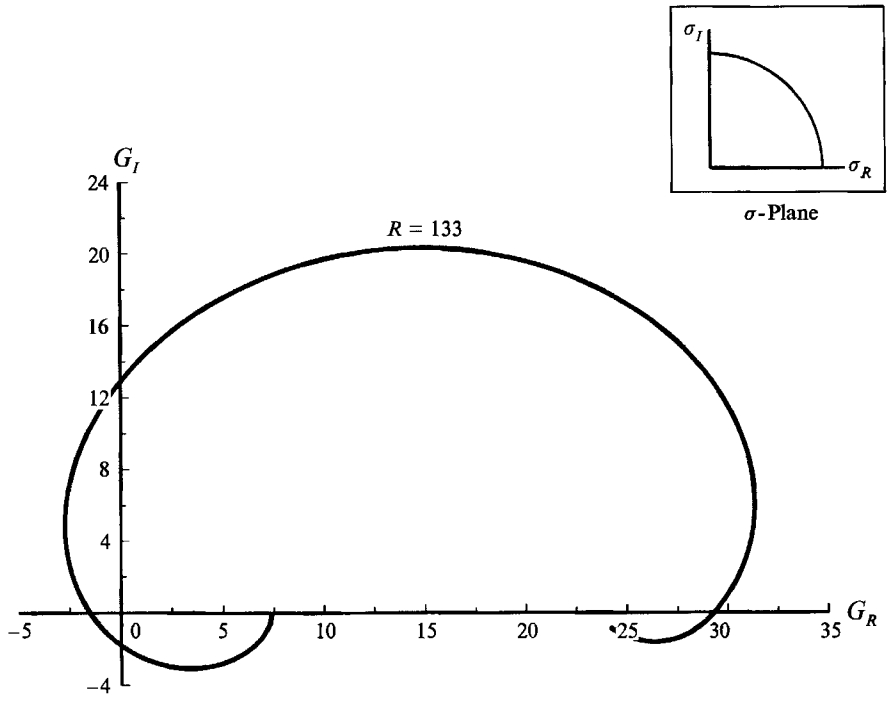

FIGURE 3. Nyquist diagram for $K_P = 4$, $K_D = 0$, $(n, m) = (1, 0)$ and $R = 133$. The map in the G-plane encircles the origin twice, suggesting the existence of two eigenvalues with a positive real part. The insert shows the contour Σ in the complex σ-plane.

5. Numerical simulation

Next, we simulate numerically the nonlinear equations of the controlled system. The numerical simulations allow us to confirm the results of the linear stability analysis in the presence of finite-amplitude disturbances.

We restrict our numerical investigation to a two-dimensional case and use the stream function and temperature as dependent variables. The partial differential equations are approximated using central differences in space and forward differences in time. We can afford to use central differences throughout (convective terms included) without being affected by numerical instabilities since we have restricted our investigation to weak convective currents. The equations are solved as an initial value problem.

To verify the numerical code, we simulate the classical, uncontrolled problem. The onset of convection is detected by carrying out a number of simulations with gradually increasing Rayleigh number. The largest R for which the no-motion state was stable and the smallest R for which the motion state was stable are denoted, respectively, by circles and squares in figure 4 and depicted as functions of the number of grid points. For a uniform mesh of 21×21 which we used in most of our simulations, the critical R at the onset of motion $R \sim 42 \pm 0.5$ (or $r \sim 1.06 \pm 0.01$, where $r = R/4\pi^2$). That is, the numerical simulation predicts a stability limit of about 6% above the linear stability theory's value. It appears that the numerical scheme introduces a slight, artificial dissipation which tends to stabilize the no-motion state. As we refine the mesh size, we are able to reduce the discrepancy between the numerically and theoretically ($4\pi^2$) determined critical value of the Rayleigh number. The supercritical-motion solution, as expected, consists of a single convective cell and is in quantitative agreement with predictions of weakly nonlinear theory.

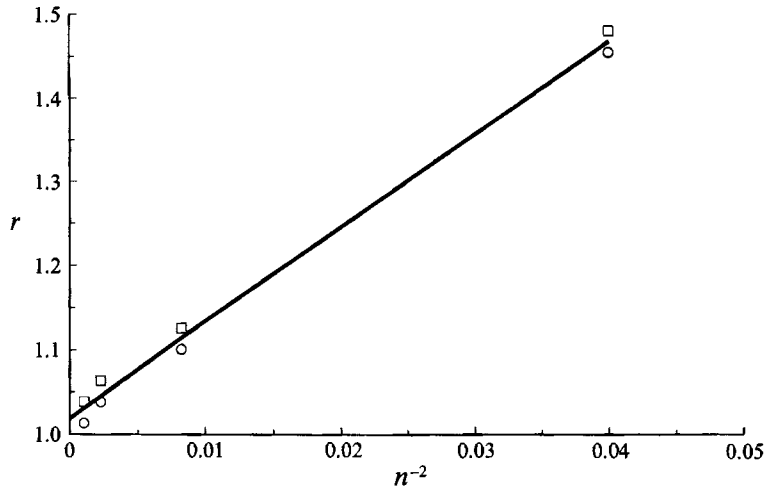

FIGURE 4. The numerical estimate for the critical Rayleigh number at the onset of convection in the classical, uncontrolled Lapwood problem is depicted as a function of the mesh size. The circles and squares correspond, respectively, to stable and unstable no-motion states.

6. Results

For conciseness, we present results only for $\chi = 0.5$, a two-dimensional square ($L_x = 1$), and a cube ($L_x = L_y = 1$). Accordingly, $(\kappa/\pi)^2 = n^2 + m^2$, where m and n are integers, and in the case of the square, $m = 0$ always. For the cube, the roles of m and n can always be interchanged owing to symmetry. Thus, whenever we say (m, n), we imply either (m, n) or (n, m).

6.1. *Marginal stability*

Figures 5–7 depict the results of the linear stability analysis. The ordinate in these figures is the relative Rayleigh number $r = R/4\pi^2$ at marginal stability. Figure 5 depicts r as a function of the wavenumber $(\kappa/\pi)^2$. Figures 6 and 7 depict, the minimal value of r from figure 5, $r_C = \mathrm{Min}_\kappa(r)$, as a function of the proportional controller's gain, K_P, for a square and a cubic cavity, respectively.

In figure 5, the dashed-dot and dashed lines respectively correspond to loss of stability via even and odd modes in the classical (uncontrolled) problem. The various solid lines correspond to controller's gains $(K_P, K_D) = (2, 0)$, $(4, 0)$, $(4.2, 0.02)$ and $(4.2, 0.06)$. The odd modes (dashed line) are not affected by the action of the controller. In the absence of a controller $(K_P, K_D) = (0, 0)$, convection sets up at $r_C = 1$ and the supercritical time-dependent, convective motion is two-dimensional and unicellular. That is, at the onset of convection, $(\kappa/\pi)^2 = 1$ corresponds to either the $(n, m) = (1, 0)$ or the $(n, m) = (0, 1)$ mode.

For $(K_P, K_D) = (2, 0)$, the growth rate of the disturbance is real and the supercritical motion is time-independent. In the case of the cube, $r_C \sim 1.76$ occurs at $(\kappa/\pi)^2 = 2$, which corresponds to $(n, m) = (1, 1)$ unicellular three-dimensional supercritical motion. In the case of the square, $(\kappa/\pi)^2 = 2$ is not admissible and $r_C \sim 1.89$ occurs at $(\kappa/\pi)^2 = 1$, which corresponds to $n = 1$ unicellular supercritical motion. Note that in both cases the controller successfully shifts the bifurcation point upwards from a no-motion to a motion state.

For $(K_P, K_D) = (4, 0)$, loss of stability occurs through an imaginary eigenvalue (Hopf bifurcation). The supercritical motion is time-periodic. In the case of the cube, $r_C \sim 3.11$ occurs at $(\kappa/\pi)^2 = 2$, which corresponds to $(n, m) = (1, 1)$ unicellular three-dimensional,

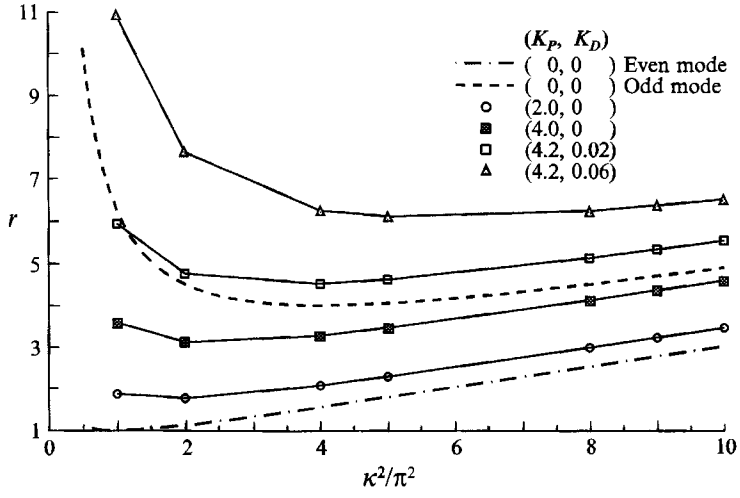

FIGURE 5. The critical normalized Rayleigh number ($r = R/4\pi^2$) at the onset of convection is depicted as a function of the wavenumber $(\kappa/\pi)^2 = n^2 + m^2$ for various values of the controller's gains. The symbols correspond to the admissible modes for the cube. The onset of convection occurs at $r_C = \mathrm{Min}_{n,m}(r)$.

supercritical motion. In the case of the square, $r_C \sim 3.27$ occurs at $(\kappa/\pi)^2 = 4$, which corresponds to $n = 2$ bicellular supercritical motion.

Unfortunately, any further increase in K_P does not yield an increase in r_C. The effects of K_P on r_C are summarized in figures 6 and 7. For $K_P < 3.85$, r_C increases monotonically with increasing K_P and the principle of exchange of stability is valid. For $K_P > 3.85$, loss of stability occurs through an imaginary eigenvalue (Hopf bifurcation). Further increases in K_P beyond 3.85 result in a reduction in r_C's magnitude as illustrated by the dash-dot line ($K_D = 0$) in figure 6.

In order to further increase the stability margin, we introduce the differential controller ($K_D > 0$). The effect of the differential controller on the marginal stability limit as a function of the wavenumber is illustrated in figure 5 for $(K_P, K_D) = (4.2, 0.02)$ and $(4.2, 0.06)$. Although at $r = 4$ the odd modes, on which the controller has no effect, are destabilized and the results presented for $r > 4$ have no practical value, the figure illustrates that the differential controller successfully increases the marginal stability of the non-odd modes.

Figure 6 depicts marginal stability results for the square cavity. The critical r-value is depicted as a function of K_P with K_D as a parameter. The figure was generated to facilitate comparison of the linear stability analysis (curves) and the numerical results (symbols). The solid and dashed curves represent, respectively, loss of stability through a real σ (exchange of stability) into unicellular ($n = 1, 0 < K_P < 2.6$) and bicellular ($n = 2, 2.6 < K_P < 3.85$) convection. The horizontal dashed line at $r = 4$ represents loss of stability through 'odd' modes which are not affected by the controller's action. The dot-dash lines represent loss of stability through an imaginary σ (Hopf bifurcation) into time-periodic bicellular convection ($K_P > 3.85$). For $K_P < 3.85$, when the principle of exchange of stability is valid, the differential controller has no effect on stability. For $K_P > 3.85$, when loss of stability occurs through a Hopf bifurcation, the differential controller (K_D) shifts upward the bifurcation point. The numbers in parentheses next to the K_D-values describe the structure of the convective motion once the critical Rayleigh number is exceeded.

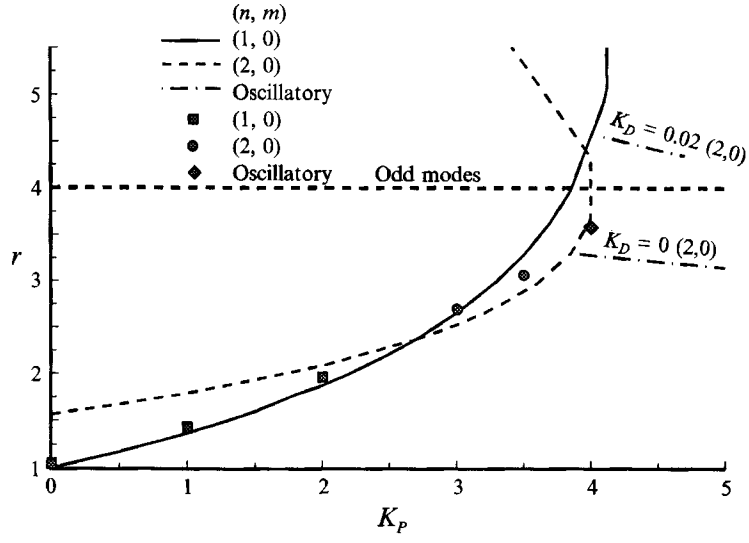

FIGURE 6. The critical normalized Rayleigh number (r) at the onset of convection in a square cavity is depicted as a function of the controller's gain K_P for $K_D = 0$ and 0.02 and for the two-dimensional modes $n = 1$ (solid curve) and $n = 2$ (dashed curve). The dashed horizontal line corresponds to bifurcation into odd modes, which are not affected by the controller's action. The lines and symbols correspond, respectively, to analytical and numerical predictions. The solid, dashed, and dot-dashed curves correspond, respectively, to bifurcation into unicellular time-independent, bicellular time-independent, and bicellular time-periodic convection.

The numerical experiments were conducted by fixing the controller's gains, introducing small temperature deviations from the conductive state, gradually increasing the magnitude of the Rayleigh number, and observing whether disturbances grow or decay as functions of time. The symbols represent the smallest values of the Rayleigh number for which non-decaying disturbances were observed. The critical numerical Rayleigh numbers were established within a precision of $\pm 2.5\%$ and they are slightly above ($< 6\%$) the analytical predictions. The solid squares, circles, and diamond correspond, respectively, to steady unicellular, steady bicellular, and oscillatory bicellular motion. The qualitative structure of the convective motion observed in the numerical experiments is in accord with the flow and temperature fields predicted by the eigenfunctions of the linear stability problem. These fields are further described in §6.3. The numerical results also suggest that the controlled no-motion state has a non-zero basin of attraction and that it can survive finite-amplitude disturbances.

Figure 7 depicts the critical r for the cube as a function of K_P for various K_D-values. The dashed and solid curves represent, respectively, bifurcation into time-independent (exchange of stability) unicellular two- $(n,m) = (1,0)$ $(0 < K_P < 1.2)$, and three-dimensional $(n,m) = (1,1)$ $(1.2 < K_P < 3.85)$ convection. The bifurcation curve (not shown) into two-dimensional bicellular convection $(n,m) = (2,0)$ is located above the $(1,0)$ and $(1,1)$ curves and will never be observed in practice. The lines labelled 'oscillatory' represent bifurcation into time-periodic convection ($K_P > 3.85$). This bifurcation can be shifted to higher r-values by engaging a differential controller ($K_D > 0$). The differential controller affects stability only when the bifurcation occurs through an imaginary eigenvalue. Note that it does not pay to increase K_P above 3.85 unless one engages the differential controller ($K_D > 0$). The 'odd modes' are destabilized

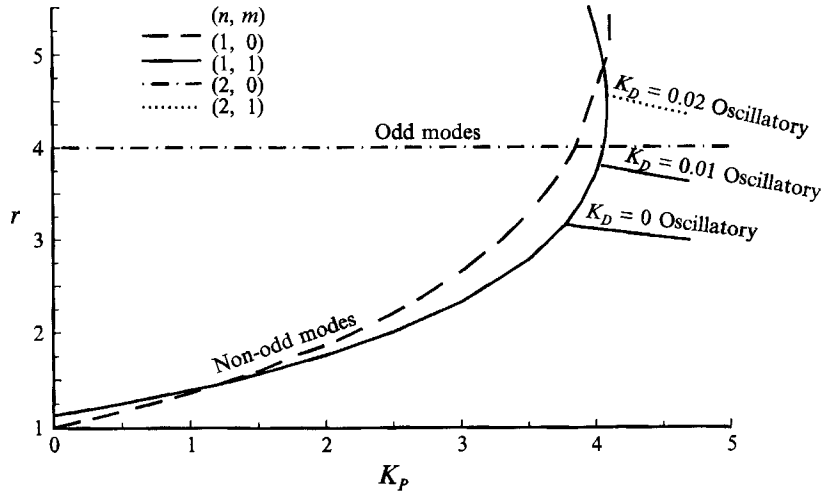

FIGURE 7. The critical normalized Rayleigh number (r) at the onset of convection in a cube is depicted as a function of the controller gain K_P for $K_D = 0$, 0.01, and 0.02. The dashed, solid, and dashed-dot lines correspond, respectively, to bifurcation into time-independent (1, 0), (1, 1) and odd modes. Lines with the label Oscillatory correspond to a Hopf bifurcation into time-periodic convection.

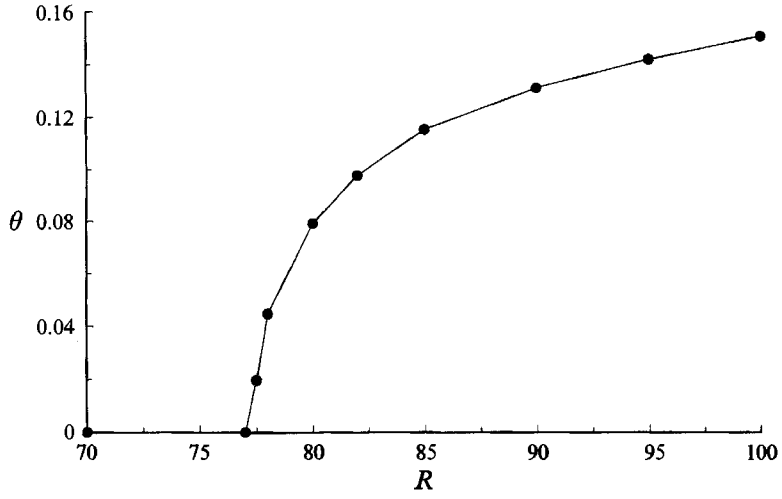

FIGURE 8. The temperature $\theta(0,0) = T(0,0) - 0.5$ is depicted as a function of the Rayleigh number for $K_P = 2$. Similar behaviour is obtained in the directions of both increasing and decreasing Rayleigh number.

at $r = 4$ (horizontal dash-dot line) which is as far as our control strategy can be used to maintain a no-motion state.

In the classical problem, loss of stability occurs through a supercritical bifurcation and the no-motion state has a global basin of attraction. Thus far, we have demonstrated that the proposed control strategy can significantly shift the onset of convection. Next, we show that, at least in the two-dimensional case, the bifurcation remains supercritical in the presence of the controller.

To this end, we conducted numerical experiments in which, for a fixed set of controller's gains, we gradually increased the magnitude of the Rayleigh number.

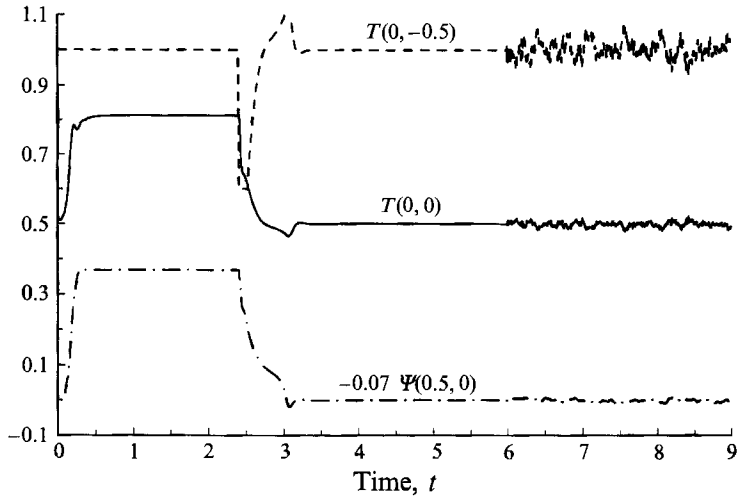

FIGURE 9. The midheight temperature at the left-hand-side lateral boundary, $T(0,0)$ (solid line); the bottom temperature at the left-hand-side corner, $T(0,-0.5)$ (dashed line); and the stream function at the box's centre, $\Psi(0.5,0)$ (dashed-dot line), are depicted as functions of time t for $R = 100$ ($r \sim 2.5$). For $0 < t < 2.5$, the controller is off. For $2.5 < t < 6$, the controller with gain $(K_P, K_D) = (3.5, 0)$ is active. The controller allows the bottom temperature to vary by no more than ± 0.4. For $6 < t < 9$, the controller counteracts the action of random disturbances.

Figure 8 illustrates the results of one such calculation for $K_P = 2$ and $K_D = 0$. $\theta(0,0)$, the difference between the steady-state temperature and its conductive value, is depicted as a function of the Rayleigh number. In the absence of motion, the temperature field is conductive and $\theta(0,0) = 0$. Once the critical Rayleigh number of the controlled system ($R \sim 77$) has been exceeded, $\theta(0,0)$ increases gradually. Other variables such as the Nusselt number (not shown here) exhibited similar behaviour. The continuous increase of $\theta(0,0)$ as a function of R, the lack of a discontinuous jump, and the lack of hysteresis suggest that the bifurcation is supercritical.

Furthermore, numerical experiments, some of which we describe in the next subsection, indicate that the controller can successfully suppress established motion. Although not a rigorous proof, this behaviour suggests, nevertheless, that the controlled no-motion state has a global basin of attraction. Large deviations from the no-motion state may, however, require large momentary changes in the bottom temperature which may cause a practical controller to saturate. Hence a practical controller may have a finite basin of attraction.

6.2. *The dynamics of the controlled system*

In this section, we describe the dynamics of the controlled system. For $R = 100$ ($r \sim 2.5$), figure 9 depicts, as functions of time t, the midheight temperature at the left-hand-side lateral boundary, $T(0,0)$ (solid line); the bottom temperature at the left-hand-side corner, $T(0,-0.5)$ (dashed line); and the stream function at the box's centre, $\Psi(0.5,0)$ (dashed-dot line). Since the convective motion in a square box consists of a single convective cell, the magnitude of the stream function at the cell's centre is a measure of the intensity of the convective motion inside the cavity. The initial conditions ($t = 0$) correspond to a no-motion state. Initially, the controller is off and the bottom temperature is uniform, $T(x,-0.5) = 1$. As a result of a thermal disturbance intentionally introduced at point $(0,0)$, clockwise motion begins. In order to contrast the controlled and uncontrolled states, we allow the motion to achieve steady state (this

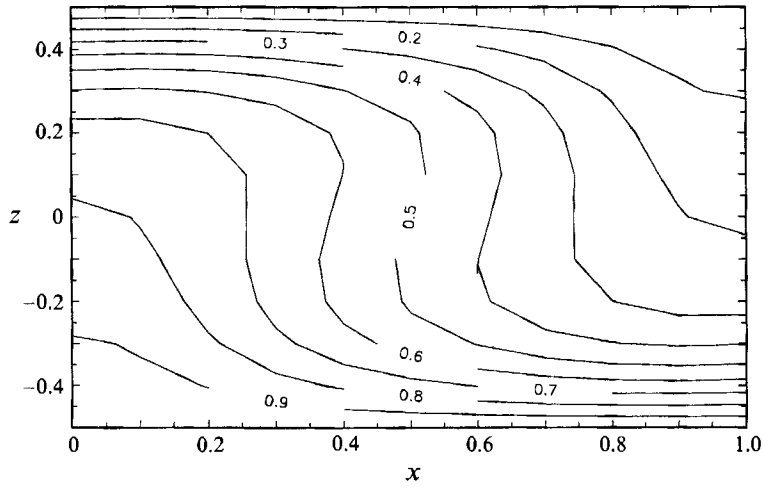

FIGURE 10. The temperature field (isotherms) associated with time-independent flow in the absence of a controller for $R = 100$.

will never happen when the controller is active). The temperature distribution (isotherms) in the cavity associated with the steady motion state ($0.5 < t < 2.5$) and consistent with unicellular convection is depicted in figure 10. Close spacing of the isotherms at the upper-left-hand-side and lower-right-hand-side corners correspond, respectively, to ascending and descending flows.

At time $t = 2.5$ in figure 9 the proportional controller with gain $(K_P, K_D) = (3.5, 0)$ is engaged (the controlled system's critical Rayleigh number for the onset of convection is 113.4). In order to simulate a realistic controller, we limited the controller's action so that it can alter the bottom temperature by at most ± 0.4. We emphasize again that in the above, for illustration purposes, we described a much more difficult task than the controller would usually confront. Most likely, in applications the controller will be switched on before the Rayleigh number has been increased and the need to suppress established motion would never arise. Since in this case we are dealing with established motion, for a short amount of time, the controller alters significantly the bottom temperature (but by less than ± 0.4) and saturates: witness the decline of the corner temperature $T(0, -0.5, t)$ for $2.5 < t < 3$. The controller successfully suppresses the motion. The fact that the controller succeeded in suppressing established motion suggests that it has a large (possibly global) domain of attraction. Once the motion has been suppressed, the controller restores the bottom temperature to its nominal uniform value of 1, the midplane temperature to its conductive value of 0.5, and the magnitude of the stream function at the box's centre to its no-motion value of zero. A glance at the temperature field (not shown here) reveals perfectly horizontal isotherms. For $2.5 < t < 6$, a stable no-motion state is sustained with boundary conditions identical to the ones of the uncontrolled system and for a Rayleigh number 2.5 times the critical one for the onset of convection in the uncontrolled system. In other words, in an ideal system, which is not subject to finite-amplitude disturbances, the controller does not alter the no-motion state; it only alters the system's dynamics.

Typically, in practice, the controller will need to cope with small random disturbances. In order to investigate the system's response to such disturbances, for $t > 6$ we introduced random fluctuations in the temperature field, varying the temperature of each grid point at each time step by random noise with maximum

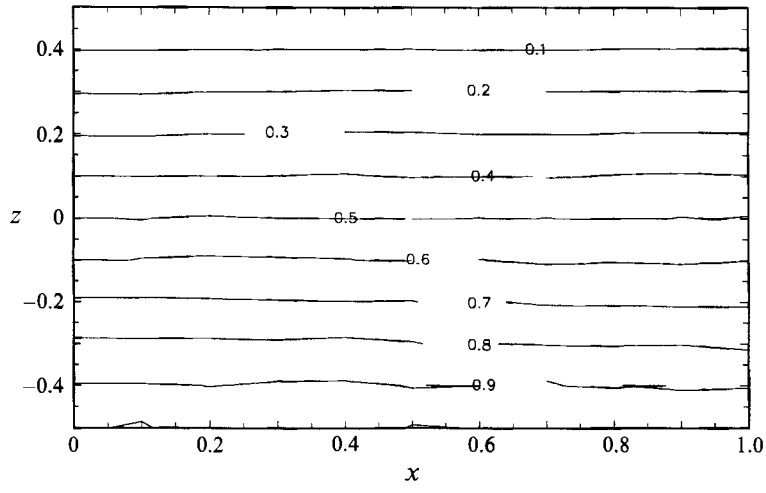

FIGURE 11. The temperature field (isotherms) for $R = 100$ in the presence of a controller with $(K_P, K_D) = (3.5, 0)$ and random fluctuations in the temperature field.

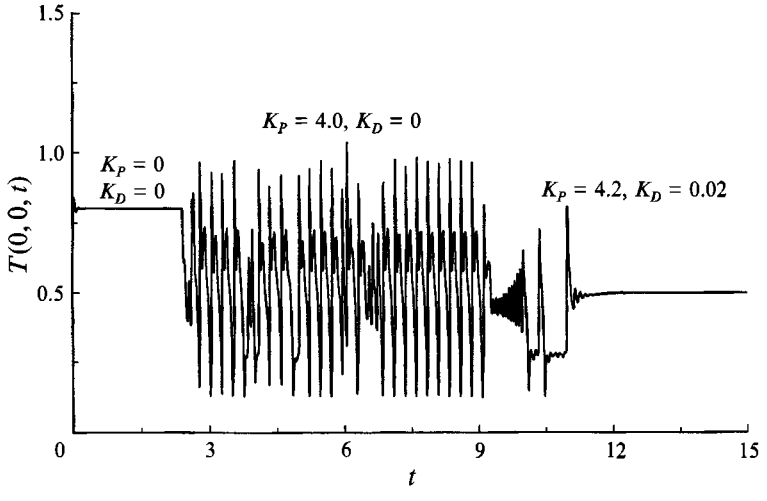

FIGURE 12. The midheight temperature at the right-hand-side lateral boundary, $T(0, 0)$, is depicted as a function of time t. $R = 150$. For $0 < t < 2.5$, the controller is off. For $2.5 < t < 9$, after initial transients die out, periodic motion is observed as a result of engaging the controller $(K_P, K_D) = (4.0, 0)$. The controller allows the bottom temperature to vary by no more than ± 0.7. At $t = 9$, the controller $(K_P, K_D) = (4.2, 0.02)$ succeeded in suppressing the motion and bringing $T(0, 0)$ to its no-motion conductive value of 0.5.

amplitude of $\pm 1\%$. Despite these disturbances, the bottom temperature remained close to its nominal value of one, the isotherms remained almost horizontal (see figure 11), and there was essentially no motion in the box. The lack of motion is signalled by the stream function's value being close to zero. Figure 11 shows a snapshot of the temperature field (isotherms) at $t = 9$ in the presence of random disturbances. Figure 11 should be contrasted with figure 10 which corresponds to almost the same boundary conditions.

Next, in figure 12, we describe the system's dynamics under conditions in which the proportional controller alone cannot suppress the convective motion. The temperature

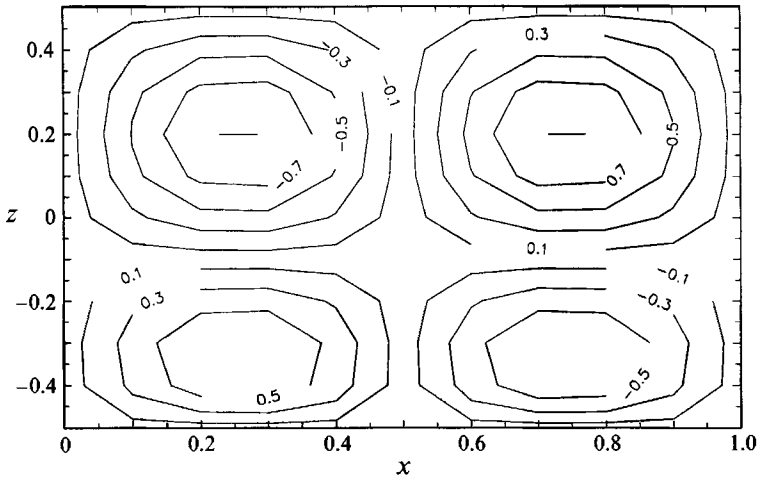

FIGURE 13. The time-independent, supercritical flow field is depicted for $R = 122$ ($r = 3.09$), $K_P = 3.5$ and $K_D = 0$. The stream-function values are multiplied by a factor of 10.

$T(0, 0)$ is depicted as a function of time t for $R = 150$ ($r \sim 3.75$). For clarity, we do not depict the bottom temperature and stream function values as we have done in figure 9. In order to contrast the uncontrolled system with the controlled one, we allow steady convection to develop while the controller is switched off ($0 < t < 2.5$). We emphasize again that this is rather an unusual situation. In a typical application, the Rayleigh number will be gradually increased from zero to a prescribed value with the controller switched on so that established motion will never occur.

At time $t = 2.4$ we engage a proportional controller with gain $K_P = 4$ and $K_D = 0$. Since the controller faces the daunting task of suppressing fully developed convective motion, the actuators will have to effectuate fairly large fluctuations in temperature at certain locations along the bottom. We have restricted these fluctuations to $\pm 70\%$. Consequently, the controller occasionally saturated. The proportional controller alone is not capable of suppressing the motion. After initial transients die out, the controlled system exhibited time-periodic behaviour. This is in accord with predictions of linear theory (figure 6). In order to suppress the motion, we engaged at time $t = 9$ both proportional ($K_P = 4.2$) and differential ($K_D = 0.02$) control. In agreement with linear theory, the combined action of the differential and proportional control is capable of suppressing the motion. Witness that the temperature $T(0, 0)$, the bottom temperature $T(x, -0.5)$, and the maximum absolute value of the stream function (not shown in figure 12) return, respectively, to their no-motion conductive values of 0.5, 1 and 0. For time $t > 12$ the isotherms are horizontal and there is no motion in the cavity. In other words, the controller maintains a stable no-motion state for Rayleigh numbers 3.75 times the critical one for the onset of convection in the uncontrolled system.

6.3. *The behaviour of the supercritical system*

The major objective of the control strategy is to shift to higher Rayleigh numbers the bifurcation point from the no-motion to the motion state. The controller affects the dynamics of the system by altering the stability characteristics of the no-motion state while preserving the boundary conditions of the uncontrolled system. In other words, as long as the critical Rayleigh number of the controlled system is not exceeded, the no-motion states of the controlled and uncontrolled systems are identical. Once the critical Rayleigh number of the controlled system has been exceeded, however, the system will

exhibit convective motion significantly different from that of the uncontrolled system with significantly different boundary data.

For example, in figure 13, we depict the steady-state flow field (streamlines) for $r \sim 3.09$. For the same Rayleigh number, the motion in the uncontrolled system consisted of a single convective cell while in the controlled system (figure 13), we observed four cells. Of course now the bottom temperatures of the controlled and uncontrolled systems are significantly different. The four-cell structure is consistent with the linear stability theory's predictions. We did not depict the temperature field since, owing to the weakness of the convection, its structure does not significantly deviate from that of the conduction isotherms.

Figures 14(*a*), 14(*b*) and 14(*c*) depict, respectively, the temperature $T(0, 0, t)$, the flow field (streamlines), and the temperature field, as functions of time for $K_P = 4$, $K_D = 0$ and $R = 150$ ($r = 3.80$). In line with the linear analysis predictions, we observe time-periodic behaviour. The various frames in figures 14(*b*) and 14(*c*) represent snapshots at various times during one period. The frames in figures 14(*b*) and 14(*c*) should be correlated with the bullets in figure 14(*a*). In contrast, for the same Rayleigh number, the uncontrolled system exhibits time-independent unicellular motion.

We included figures 13 and 14 to illustrate that once the critical Rayleigh number of the controlled system has been exceeded, the resulting motion is significantly different from that in the uncontrolled system. Figures 13 and 14 demonstrate, however, yet another potential application of a controller. Instead of preserving equilibrium states of the uncontrolled system, the controller can be used to adjust the boundary conditions in such a way as to achieve desired flow behaviour unavailable in the uncontrolled system. For example, in certain applications, the flow structure depicted in figure 13 may be superior to the unicellular convection of the uncontrolled system since it is less effective in transporting contaminants from the bottom boundary to the top one.

7. Conclusions

We have demonstrated that feedback control can be effectively used to stabilize the no-motion state of a saturated porous layer heated from below. More specifically, with the use of a simple controller, one can increase the critical Rayleigh number for the onset of convection by as much as a factor of 4. Additional gains could possibly be made through the use of more elaborate controllers than the ones we have considered here.

In essence, without affecting the classical equilibrium state, the controller modifies the system's dynamics by enhancing the disturbance dissipating mechanisms in the fluid. In a system subject to finite-amplitude noise, the controller will maintain the no-motion state through small modulations in the boundary temperature. In such a case, the isotherms will be almost horizontal. Once the Rayleigh number exceeds the critical one for the controlled motion, the resulting supercritical flow will significantly differ from that in the uncontrolled system. This suggests yet another application of the controller, which was not explored in this paper. Rather than stabilizing an equilibrium state of a given system, the controller could be used to create new flow structures, optimized in such a way as to suit particular process requirements.

Control strategies similar to the one described in this paper can also be used to delay the onset of convection in the Rayleigh–Bénard problem (Tang & Bau 1993).

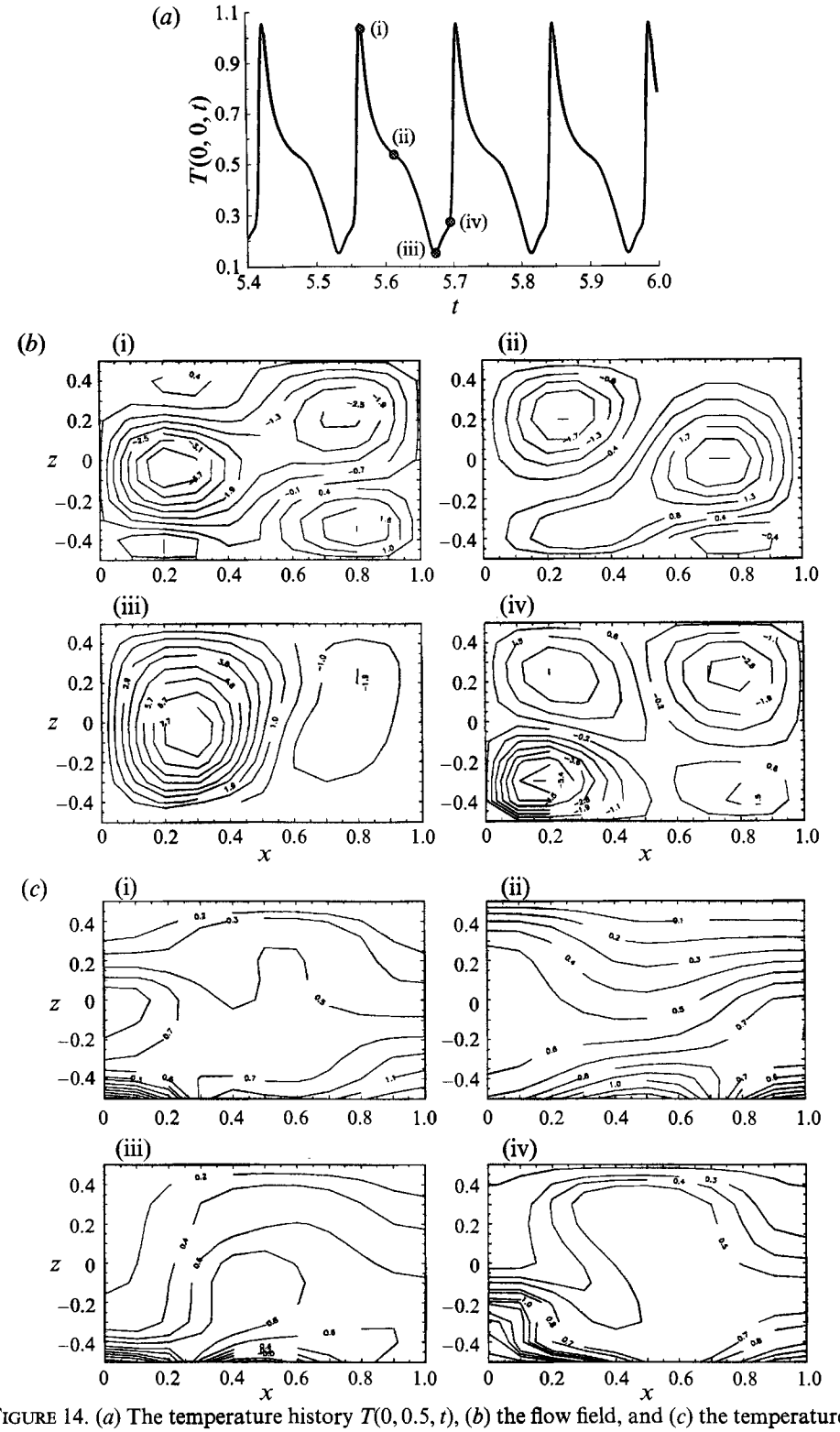

FIGURE 14. (*a*) The temperature history $T(0, 0.5, t)$, (*b*) the flow field, and (*c*) the temperature field are depicted as functions of time for $R = 150$ ($r = 3.8$), $K_D = 0$, and $K_P = 4$. The frames in (*b*) and (*c*) are snapshots at various times during the period and should be correlated with the bullets in figure (*a*).

This work was supported, in part, by the Department of Energy, Office of Basic Energy Sciences, through Grant DE-FG02-92ER14271. The numerical simulations were conducted, in part, using the Cornell National Supercomputer Facility. We are grateful to Professor Doedel for providing us with the software package AUTO. Preliminary reports of parts of this work were given in Tang & Bau (1992) and Bau (1992).

REFERENCES

BAU, H. H. 1992 Controlling chaotic convection. In *Theoretical and Applied Mechanics 1992* (ed. S. Bonder, J. Singer, A. Solan & Z. Hashin), pp. 187–203. Elsevier.

BAU, H. H. & TORRANCE, K. E. 1982 Low Rayleigh number thermal convection in a vertical cylinder filled with porous materials and heated from below. *Trans. ASME* C: *J. Heat Transfer* **104**, 166–172.

BECK, J. L. 1972 Convection in a box of porous material saturated with fluid. *Phys. Fluids* **15**, 1377–1383.

CARRIER, G. F., KROOK, M. & PEARSON, C. E. 1966 *Functions of Complex Variables – Theory and Techniques.* McGraw-Hill.

DAVIS, S. H. 1976 The stability of time periodic flows. *A. Rev. Fluid Mech.* **8**, 57–74.

DOEDEL, E. 1986 AUTO: software for continuation and bifurcation problems in ordinary differential equations. *Applied Mathematics Rep.*, California Institute of Technology.

DONNELLY, R. J. 1990 Externally modulated hydrodynamic systems. In *Nonlinear Evolution of Spatio-Temporal Structures in Dissipative Continuous Systems* (ed. F. H. Busse & L. Kramer), pp. 31–43. Plenum.

JOSEPH, D. D. 1976 *Stability of Fluid Motions II.* Springer.

KATTO, Y. & MASUOKA, T. 1967 Criterion for onset of convective flows in a fluid in a porous medium. *Intl J. Heat Mass Transfer* **10**, 297–309.

KELLY, R. E. 1992 Stabilization of Rayleigh–Bénard convection by means of a slow nonplanar oscillatory flow. *Phys. Fluids* A **4**, 647–648.

LAPWOOD, E. R. 1948 Convection of fluid in a porous medium. *Proc. Camb. Phil. Soc.* **44**, 508–521.

MEYER, C. W., CANNEL, D. S. & AHLERS, G. 1992 Hexagonal and roll flow patterns in temporally modulated Rayleigh–Bénard convection. *Phys. Rev.* A **45**, 8583–8604.

ROPPO, M. N., DAVIS, S. H. & ROSENBLAT, S. 1984 Bénard convection with time-periodic heating. *Phys. Fluids* **27**, 796–803.

SINGER, J. & BAU, H. H. 1991 Active control of convection. *Phys. Fluids* A **3**, 2859–2865.

SINGER, J., WANG, Y.-Z. & BAU, J. H. 1991 Controlling a chaotic system. *Phys. Rev. Lett.* 66, 1123–1125.

TANG, J. & BAU, H. H. 1992 Stabilization of the no-motion state of a horizontal, saturated porous layer heated from below. In *Stability of Convective Flows* (ed. P. G. Simpkins & A. Liakopoulos), ASME-HTD-219, pp. 23–30.

TANG, J. & BAU, H. H. 1993 Stabilization of the no-motion state in Rayleigh–Bénard convection through the use of feedback control. *Phys. Rev. Lett.* **70**, 1795–1798.

WANG, Y.-Z., SINGER, J. & BAU, H. H. 1992 Controlling chaos in a thermal convection loop. *J. Fluid Mech.* **237**, 479–498.

WOLFRAM, S. 1991 *Mathematica, A System for Doing Mathematics by Computer.* Addison-Wesley.